Modeling floating object entry and exit using smoothed particle hydrodynamics

Cited As:

Vandamme, J.*, Q.-P. Zou, and D. E. Reeve, 2011: Modelling floating object entry and exit using Smooth Particle Hydrodynamics, ASCE, *J Waterway, Port, Coastal and Ocean Engineering*, Vol 137, Issue 5, pages 213-268, https://doi.org/10.1061/(ASCE)WW.1943-5460.0000086

Modelling Floating Object Entry and Exit Using Smoothed Particle Hydrodynamics

Johan Vandamme[1], Qingping Zou[2] and Dominic E. Reeve[3]

ABSTRACT

This paper investigates fluid and floating object interaction using a novel adaption of the Weakly Compressible Smoothed Particle Hydrodynamics (WCSPH) method by incorporating a floating object model. In particular, this paper examines the water impact, hydrodynamic forces, fluid motions and movement of objects in the conventional case studies of object entry and exit from still water. A 2D wedge drop analysis was examined, and the water impact pressure prediction, traditionally considered one of the weaker facets of WCSPH, shows good agreement with published experimental and numerical results. The hydrodynamic forces exerted on the object, and hence the movement of the object itself, are both well predicted. The velocity field of the fluid domain is also captured well. Simulations for water entry and exit of a buoyant and neutral density cylinder compares well with previous experimental, numerical and empirical studies in penetration, free surface comparisons and object movement. These results provide a good foundation to evaluate the accuracy and stability of WCSPH for modelling the interaction between free surface flow and free moving floating objects.

Keywords: Smoothed Particle Hydrodynamics, Object Entry, Object Exit.

1.0 INTRODUCTION

The study of interactions between fluid and floating object, although a challenging subject area in its own right, has become a more pressing practical problem with the increase in demand for wave energy extraction, and offshore explorations. Many of the objects designed will be placed in high sea states, and subsequently they must be designed to withstand the forces arising from extreme wave conditions. Numerical modelling of this type of situation could prove a cost effective method for simulating such conditions, not suffering from the scaling problems present in physical models. Due to the anticipated range of structures and wave conditions, it is important that the numerical technique is accurate and robust.

Although there are many methods of numerical simulation for wave dynamics, including the modelling of floating objects, (Greenhow and Moyo 1997; Zhao et al. 1997; Yan and Ma 2007; Zhang et al. 2010) the traditional methods of modelling are

[1] Centre for Coastal Dynamics and Engineering, School of Marine Science and Engineering, University of Plymouth, Drake Circus, Devon, PL4 8AA, UK. E-mail: johan.vandamme@plymouth.ac.uk
[2] Centre for Coastal Dynamics and Engineering, School of Marine Science and Engineering, University of Plymouth, Drake Circus, Devon, PL4 8AA, UK. E-mail: Qingping.zou@plymouth.ac.uk
[3] Centre for Coastal Dynamics and Engineering, School of Marine Science and Engineering, University of Plymouth, Drake Circus, Devon, PL4 8AA, UK. E-mail: Dominic.reeve@plymouth.ac.uk

grid based. These methods subsequently encounter a marked increase in computational difficulty when phenomena such as flow separation, vortex shedding, surface piercing, flow coherence or large differential movement are involved in the simulation. As a result, it becomes increasingly difficult to accurately capture the movement and fluid response to a floating object.

The increasing computational power that is available to researchers has meant that numerical methods have evolved beyond the Eulerian grid-based methods of modelling. The computational method presented in this paper is particle based; creating a dexterous mesh-free numerical modelling technique.

Initially developed for the study of the particle motion in highly turbulent scenarios within astrophysics by Gringold and Monaghan (1997) and Lucy (1997), Smoothed Particle Hydrodynamics (SPH) has been adapted for free surface flows and other hydrodynamic problems; (Monaghan 1994; Monaghan 2000; Gómez-Gesteira and Dalrymple 2004; Gómez-Gesteira et al. 2005; Dalrymple 2007; Rogers et al. 2008; Dalrymple et al. 2009; Ferrari 2010; Gómez-Gesteira et al. 2010).

Developments of the SPH method have recently diverged towards new formats and methods of with subsequent reduction in CPU demands, including a GPU (Hérault et al. 2010) and a parallelised version (Ferrari et al. 2009) of SPH. The fundamental processes of WCSPH, however, have not changed significantly, with only slight additions to the hydrodynamic pressure evaluation, (Molteni and Colagrossi 2009) and changes to the angular momentum conservation, (Ataie-Ashtiani and Mansour-Rezaei 2009).

With WCSPH, the pressure values of the fluid particles are dependent on the change in density and a state equation, which can cause large pressure fluctuations, as noted by Xu, Stansby et al. (2009). This inaccuracy can be reduced by re-meshing the particles across a uniform grid as proposed by Chaniotis et al. (2002), but this subsequently contravenes the mesh-free nature of SPH and thus is not used in this paper.

In this study, we developed an extra module to simulate the movement of solid bodies within the SPH program. To achieve this, an object is considered to be composed of solid boundary particles, their local positions fixed relative to each other, and their global positioning dependent on the hydrodynamic forcing of the water particles which act normally to the obstacle surface. This approach is different from the work of Ataie-Ashtiani and Mansour-Rezaei (2009) where the SPH modelling of an object movement is pre-defined and does not respond to any hydrodynamic conditions.

This approach presents a convenient method with which to model many types of floating objects within many different situations. Within this paper, we extend the research of modelling floating objects with SPH by examining the full range of object movements using a standard and continuous particle placement, using regular

spacing of the fluid particles, in contrast to the complex initial radial particle spacing of Oger et al. (2006)

The objective of this present study is to combine the floating object movement prediction model with the SPH model to investigate the interaction of flow and floating objects. The model results are then compared with benchmark test cases of water entry and exit, or wedges and cylinders. Pressures and velocities are compared with published results.

2.0 SPH MODELING

The mathematical basis for the SPH method is modelling the fluid domain as a number of discrete particles whose interactions are based on the Navier-Stokes equations. The representation of the fluid domain as particles uses a Lagrangian approach that allows the detailed examination of fluid responses. As explored in the previous section, SPH has been used in a variety of free turbulent surface flows.

The main form of SPH is Weakly Compressible SPH, although a fully incompressible methods (ISPH) have also been developed e.g. (Shao and Y.M.Lo 2003; Shao et al. 2006). Although ISPH tends to predict pressure fluctuations more accurately, the overall results of both methods are often comparable. Run times for identical numerical models are similar, as the ISPH method takes longer per time step but will use larger time steps throughout the run. WCSPH allows for a smaller particle size, giving a higher resolution, for any given memory size (Colagrossi and Landrini 2003). It is the WCSPH method that is used in this paper.

2.1 HYDRODYNAMIC MODEL

Once an initial geometry is defined, the particles that have been created in the numerical domain are assigned scalar parameters that include mass, pressure, velocity components and so on. The values of these properties for all the particles can then be interpolated to compute any one of the scalar quantities for any given particle, using a smoothing function which is known as the kernel function.

The conservation of momentum and mass, as shown by Monaghan in his (1994) paper, is applied to the particle *a* in the form:

$$\frac{dv_a}{dt} = -\sum_j m_j * \left(\frac{p_a}{\rho_a^2} + \frac{p_j}{\rho_j^2} + \prod_{aj}\right) \nabla_a W_{aj} + g \qquad (1)$$

$$\frac{dp_a}{dt} = \sum_j m_j \left(v_a - v_j\right).\nabla_a W_{aj} \qquad (2)$$

where *j* is all other particles within the active kernel function radius of *2h*, p_j is the pressure; v_j is the velocity; m_j the mass and ρ_j the density of particle *j*. $\prod_{aj}$ is an empirical approximation of the viscosity effects (Monaghan 1994) and W_{aj} is the kernel function.

The method used by the authors is an extension of WCSPH, which has been further developed by the authors from the open-source SPHYSICS code (v1.0.002) published on the University of Manchester website (SPHYSICS 2008) by developing a method to model the feedback between moving objects and fluid motion, as described in the subsequent sections. In this weakly compressible approach, the compressibility is simulated by altering the density of the particles, and subsequently calculating their volume. Conservation of mass is guaranteed therefore, providing that no particles enter or leave the numerical domain.

The development of SPH is well documented, for example, in (Dalrymple and Rogers 2006), and therefore not described in great detail here. The model version used here includes the XSPH correction (Monaghan 1989), and the kernel functions used have been integrated with artificial pressure to correct tensile instability as shown in Dyka and Ingel (1995), Dyka et al. (1997), and Monaghan (2000) Sub-particle turbulence is modelled after Dalrymple and Rogers (2006) and Morris (1996). Execution time of the modelling has been decreased by using the linked-list, as suggested by Viccione et al. (2008). WCSPH uses a self-correcting time step, and as such this is not listed in the parameters used for each case study in this paper.

2.2 SOLID PARTICLES MODEL

The boundaries of the numerical domain in the SPH method are constructed from particles according to the domain geometry. These particles have their position defined, either as fixed in space or moving with a specified function in time, for example a paddle wave maker. These particles are then included within the kernel integration and will exert proportional repulsive forces in opposition to the movement of a fluid towards the boundary. The two main approaches of modelling the boundary particles are set out by Monaghan (1994), and by Gómez-Gesteira et al. (2005).

The mechanisms of floating object modelling within the SPH simulation has been achieved by using solid particles to construct the shape of the object in question. In contrast to the method employed by Campbell et al. (2008), this allows a homogeneous method of computation, and improves the efficiency of the model. The effect of the floating object particles on the fluid is included within the kernel function, but the hydrodynamic forcing onto the floating object particles is computed independently, in the predictor-corrector mechanism of the timestep marching method. The average pressure of the fluid particles on the object surface over the previous timestep is then translated to a force by considering the fluid particles within the kernel function and the obstacle geometry. The gravitational force on the object is applied using the initial weight input, instead of the combined weight of the particles, so that a hollow obstacle can represent a solid one, and thus saving some computational time.

The net forces on the object are found through integrating the pressure field of the fluid surrounding the object particles, as shown in the equations below.

$$Fx = \sum_j p_j a_j * Nx_j \tag{3}$$

$$Fz = \sum_j p_j a_j * Nz_j + g * m_{obs} \tag{4}$$

Where *Fx* and *Fz* are the components of the force on the object in the *x* and *z* directions respectively, the particles *j* are those that make up the object, m_{obs} is the total mass of the object, and p_j, a_j and Nx_j, Nz_j are the pressures, surface area and normal component in the *x* and *z* directions of the *j* particle respectively.

The model uses the same kernel function and smoothing length as the fluid, to ensure consistency between the two phases. In addition, the authors found that numerical stability increased when the boundary particles were placed within the initial domain "grid" spacing, as this prevented obstacle particle cluster. The normal vectors for the model were derived from the initial geometry to avoid errors in computing the normal vector of the floating object after the particles had been subject to slight movement caused by the discretization. However, this can result in an apparent visual inconsistency regarding the distance from the fluid to the obstacle, but this problem is minor, and subsequently reduces with increased resolution.

Due to the rapid change in parameters of the fluid domain, and the slower response of the object, to save computational time, the movement of the object is calculated over a longer timestep than the fluid motion, in contrast to the method applied by the SPHYSICSv2.0 code, which updates at every timestep. The forces and pressures on the obstacle are then considered over ten time steps, and the object movement is computed for the longer time period, as seen in equation (5), where dt_{obs} is equal to ten times the timestep used for the fluid domain.

$$\frac{dv_{obs}}{dt_{obs}} = -\frac{F_{obs}}{m_{obs}} \tag{5}$$

2.3 MODEL COUPLING

In addition to the forces of the fluid on the obstacle, a subroutine has been developed that allows the obstacle to be anchored by one or multiple elastic mooring lines, which have a definable two part stiffness as shown below.

If $d_m \leq d_{m1}$ then

$$\overrightarrow{F_m} = -k_{m1}.\overrightarrow{d_m} \tag{6}$$

If $d_m > d_{m1}$ then

$$\overrightarrow{F_m} = -k_{m2}.\overrightarrow{d_m} \tag{7}$$

Where d_m is the displacement of the mooring point on the obstacle to the anchor point within the domain, and d_{m1} is the displacement corresponding to a change in spring constants, such that k_{m1} is the stiffness at small displacement, which could be used to represent the elastic stiffness, and k_{m2} is the stiffness at a larger displacement, which could be used to represent the plastic phase of a mooring. This method also allows an anchor such as a chain, with insignificant initial stiffness, and considerable stiffness at greater displacements, to be modelled.

The mooring forces are thus computed explicitly, and the fluid forces are found by integrating the pressure field, using the localised kernel function over the obstacle boundary particles. The sum of the fluid and mooring forces on the obstacle translate into movement of the obstacle using Newtonian mechanics. Although this requires an assumption of constant acceleration, the typical timestep of WCSPH simulations are less than 1 microsecond, and subsequently this does not result in any significant inaccuracy.

3.0 RESULTS

Results are presented for a variety of cases inherent to modelling the physical processes in the behaviour of floating objects within the developed WCSPH code. Initially, results are shown for the wedge submersion into a still fluid, both at a forced constant velocity, and as a free falling velocity dependent on the hydrodynamic response. Secondly, the method is used to examine forced cylinder entry and exit, and finally free object movement when a buoyant cylinder is placed in still water.

3.1 WEDGE ENTRY

The initial test is a case study of object entry into a still fluid. This case consists of a 2D wedge being immersed into a fluid at rest, and was first published by Greenhow (1987). Wedges with deadrise angles of 30^o and 45^o were plunged through the water surface at a constant speed of $2ms^{-1}$, capturing the surface elevation. The cubic-spline kernel function was used, with a smoothing length of 0.92, the shepard filter, and a Laminar viscosity of $1x10^{-6}$. The deadrise angle is the angle between the side of the wedge and the horizontal. Figure 1 shows the photographs of the experiment (Greenhow 1987) and the corresponding WCSPH numerical simulation.

Figure 1 serves to demonstrate the suitability of SPH for moving object interaction with fluid modelling. The size and direction of the jets are reproduced well considering the resolution of the solution. The jets and splash are underestimated due to the particle size and discretization, as variation of the viscosity showed little effect on the result. However, even with a particle diameter of 0.0025m, the computational time of the simulation still took 22 hours to run 0.1s of simulated time, on a single 2.4GHz processor, and thus higher resolutions are not feasible at this stage. The 30^o wedge produces jets which are angled much closer to horizontal than the 45^o wedge, as expected. Another apparent advantage of using a particle method such as SPH in numerical simulations of cases such as this is the ability to

allow for fluid separation, such as spray, as seen on the left-hand side of the 45^{o} wedge. This phenomena is much more complex for a computational method that uses grids or meshes in place of particles.

This test case shows the accuracy when considering a simplified case with a defined movement and a still fluid. In reality, any design for a floating object would be required to model the object response to the fluid as opposed to the case in Figure 1 which constrains the velocity to a constant throughout the test. As such the following test shows the results of a wedge plunging into the fluid at a defined entry velocity, wherein the subsequent wedge movement is a result of the fluid forces on the intruding object. There are plenty of examples of physical and theoretical testing around the subject area of wedge slamming, which is important to not only the renewable energy industry but also the shipping and ocean transport industry. Aside from Greenhow (1987), extensive work has been carried out by Zhao and Faltinsen in (1993) and (1997) considering the entry of arbitrarily shaped 2D bodies, as well as the impact study of Cointe (1987) and the detailed vertical and oblique entry of wedges presented by Judge et al. in (2004).

Figure 2 shows the sequence of images with the wedge (with a 30^{o} deadrise angle) plunging into the still water. The initial penetration into the surface cases the fluid to move down and to the side of the incoming wedge. These jets are attached to the wedge surface and propagate further up as the wedge progresses deeper into the fluid domain. Eventually the jets detach from the wedge surface and shoot to the side as seen in the final image. The maximum velocity of the jets is 17.1ms^{-1} in the final image, being 15.8ms^{-1} in the second image. These values compare well with the values predicted numerically with the previous research (Oger et al. 2006; Shao 2009).

The second test is of a wedge with an entry velocity of 6.15ms^{-1}, and the results are compared with those published by Shao (2009) who used ISPH with an identical resolution to that of the authors. The cubic-spline kernel function was again used, and the viscosity was Laminar & SPS method, with a v value of 8x10^{-7}. The run time for 0.4s of simulation time was 25 hours. The results show the water surface elevation, fluid domain velocity vectors and pressure contours for the time following the initial impact.

The top panel of Figure 3 shows the close correlation between the velocity predictions of weakly compressible SPH results and the existing ISPH results. The RMSE error of the predicted velocities to the measured value is 0.36%. The velocity of the WCSPH wedge closely follows the expected trend and gives a much smoother profile than the results shown by Kleefsman (2005), and the results sit comfortably within the data points measured by Zhao et al. (1997). Towards the maximum time values measured there is a slight inaccuracy where the simulated results decelerate more slowly than the other results, however this is still well within reasonable tolerance.

The bottom panel of Figure 3 shows the force prediction, a factor that is often considered the least accurate parameter of WCSPH. The pressure of the fluid is affected by the kernel function, but the smoothing length has a slight effect on the force, although the test case (with h=0.95) was nonetheless under predicted. Although the initial rise in upwards force seems languid, this appears to be the result of the pressure wave moving away from the obstacle resulting in a slight underestimation of the fluid pressure. The smoothing length had no real bearing on this effect. The peak and residual forces are predicted correctly and the profile of the results are well matched, with a RMSE between the predicted pressure and the measured ones of 12.4%.

Pressure oscillations within WCSPH, as shown in Figure 3, are not uncommon (Gong et al. 2009), and although they are not a source of significant error due to their high frequency and low amplitude, research is still ongoing to correct the problem (Molteni and Colagrossi 2009). The slight oscillations within the results are likely to be the result of a slight feedback resulting from the timestep and sound wave speed used, causing a feedback between pressure waves, or could be caused by the different timesteps used within the method. Nonetheless, these do not significantly affect the prediction of the movement of a floating object, which is evaluated at a longer timestep than the fluid response. In addition, the force was extracted at specific time periods, without the averaging over the 10 time steps, which could have smoothed the profile significantly.

The decrease in force is significantly steeper than the other predictions, which is believed to be caused by the pressure wave radiating out at a higher velocity than the wedge, causing a more sudden drop in the pressure of the particles at a close proximity, which has a high impact on the pressure integration due to the shape of the cubic-spline kernel function that was used.

Although it is traditionally viewed as one of the weaknesses of weakly compressible SPH, the pressure induced in the entire fluid domain can be compared with the ISPH results, as shown in Figure 4. The two sets of data were computed using identical particle sizes (diameter = 0.01m).

The upper image of Figure 4 clearly shows a bulb of high pressure under the initial impact of the wedge, with no disturbance to the fluid further afield. The ISPH has a faster response time for pressure variations due to the incompressible nature, which may be why the highest pressure is at the surface instead of below the nose of the wedge. The maximum pressure under the wedge is in the region of 100kPa. This area of high pressure diffuses as the water moves upwards and sideways along the wedge, as shown in the second figure where the maximum pressure is around 70kPa.

An obvious discrepancy between the two sets of results is displayed in the second time step shown in Figure 4, where the surface profile of the ISPH model already

displays some splashing and a more significant jet formation than the authors' results, which show a more uniform fluid surface which forms a jet later in the simulation, producing a more powerful jet than the ISPH. This is logical, considering the instantaneous pressure transfer in ISPH compared to the sound wave dependent WCSPH.

The discretized nature of the particle model presents difficulties when computing the prediction of jet volume, so it is hard to know which result is more accurate. However, the authors result predicts a more powerful jet than the ISPH results, where are understood to be significantly weaker than those found in Oger et al. (2006). The methodology used in the work by Oger et al. (2006) is based on the weakly compressible SPH method, however the initial conditions were altered to give a complex radial spacing and variable resolution, affording a very fine resolution at the surface to try to predict the jets accurately.

The results of the 30^o wedge entry shows the performance of a normally configured weakly compressible SPH in predicting the fluid forces upon an object and also the forces within the fluid domain itself. This is a crucial step towards modelling a floating object over longer time periods, where there will be inevitable instances of exit and/or entrance into the fluid surface by the object.

We have also examined the slamming coefficient for various wedge angles, for which there are fewer results for comparison. Figure 5 shows some initial results of slamming coefficients for wedges of 30^o, 45^o, and 60^o deadrise angles, using the same computational conditions as for Figures 1 and 2. The results are compared against the theoretical predictions of Greenhow (1987), Borg (1959) and Wagner (1932).

The slamming coefficient comparison in Figure 5 shows that the WCSPH model tends towards the trend and peak values of slamming well. Although there is some noise within the results, this does not detract from the overall similarities.

3.2 CYLINDER ENTRY

Also considered are the free surface profiles caused by a free velocity cylinder dropped into calm water. Cylinders of density $500kgm^{-3}$ and $1000kgm^{-3}$, with diameter of 0.11m are dropped through a distance of 0.5m, until they reach the water surface. The water depth is 0.30m. Both simulations were run with a cubic-spline kernel, and the smoothing length was 0.9. The Lamiar & SPS viscosity method was used with a v value of $1x10^{-6}$, and the resolution used was 0.0065. Results are compared to the experiments of Greenhow and Lin (1993) and the CIP (Constrained Interpolation Profile) method of Zhu et al. (2007).

Figure 6 shows the surface movement resulting from the impact of the $500kgm^{-3}$ cylinder on the water surface. It can be seen that the impact of the cylinder causes a jet on each side to be formed, and this jet appears to flow in a more vertical direction

as the cylinder continues into the fluid. In addition to this, the flow separation as the cylinder keeps plunging is also well predicted with the WCSPH method, with the water surfaces on either side being straighter, and closer to the experimental data than the CIP method (Zhu et al. 2007).

Due to the same discretization problem that was experienced in the wedge entry, the jets are not as accurately calculated as the experimental results show, however, simulating a run of 1s took over 6 hours, and a resolution high enough to accurately capture the jet phenomena would require excessive computational resources.

The penetration depth of the cylinder can be seen in Figure 7. This shows an excellent agreement with the experimental data for the first 0.4 seconds. The apparent over prediction of the penetration compared to the experimental data is also reflected in the CIP method, and at this stage it is not clear why this discrepancy occurs.

Figure 8 shows the images of a cylinder with density of 1000kgm^{-3} being dropped into the fluid. As the WCSPH model does not include an air phase, the speed of impact is identical to the previous test. This cylinder penetrates to a much deeper level, reaching the bottom of the tank at t=0.50s. The method used by Zhu et al. (2007) was to reflect the velocity of the cylinder upwards upon contact with the boundary particles, which is the same method used by the authors due to the reflective nature of the boundary particles.

The slight particle clumping that can be seen in Figure 8 is a longstanding problem in the WCSPH method. Measures to minimise particle clumping, such as XSPH (Monaghan 1989), artificial stress within the kernel function (Monaghan 2000) and recent research in viscous fluids (Fang et al. 2009) has gone some way to address the problem. However, the unphysical particle clumping is caused by the shape of the kernel function, and the gradient of the kernel function when the particles are in close proximity is too slight (Vaughan et al. 2008). As a result of this, reducing the smoothing length, and subsequently the kernel function minimises the effect.

The initial image shows the formation of the jets and the flow separation around the side of the cylinder. As the progression through the simulation continues, the free surface becomes more fragmented, as evidenced by the layers of yellow and green in the results of Zhu et al. (2007), and by the disordered scatter of the particles in the authors' WCSPH method. Both methods seem to predict the angle of the jets at 0.110 seconds to be angling inwards more than the experiment shows, however the WCSPH method is closer to the experimental data.

It is evident from Figure 6 that the cylinder particles are within the initial "grid" spacing, and as such the representation is not entirely circular. This is because when a completely circular obstacle was created without using the regular spaced particles, the model suffered regular instabilities. The particles are aligned to the initial grid, but retain the normal vector of the cylinder. However, this contributes to

an increase in the separation between the fluid and the location of the grid points where the particles are displayed. This effect is reduced substantially with higher resolutions (Ataie-Ashtiani and Mansour-Rezaei 2009).

The final two images show the water surface closing over the submerged obstacle. The shape of the water surface is well predicted by the WCSPH method, including the near-vertical jets continuing at 0.200 seconds, and the height of the cumulating water column at 0.450s.

Figure 9 shows the penetration depth of the cylinder after the initial impact at 0.3 seconds. The WCSPH results are closely correlated to the CIP results, which sit in reasonable correlation between the experimental data points. The experimental result at 0.34 seconds appears to be slightly anomalous, considering the latter points.

3.3 CYLINDER EXIT

The exit of an object from the fluid domain is critical to the design of floating objects and wave energy converters. The behaviour of an obstacle exit, however, has significantly less published research available for comparison, but some test cases have been modelled and the results are shown below.

When a cylinder is submerged into the fluid domain and forced to rise through the surface of the fluid, the free surface deformation has been presented by Greenhow and Moyo (1997) and is compared to the SPH numerical results in Figure 10. This test case involved a cylinder of diameter 0.5m with a density of 1000kgm^{-3}, and was submerged at a depth of 1m before being forced to rise at a constant motion of 1ms^{-1} upwards. The particle size was 0.02m, and the simulation was run using a cubic-spline kernel of smoothing length 0.85, and a Laminar & SPS viscosity (ν) value of 1x10^{-6}. The smoothing length is as short as feasible to minimise clumping and discretization effects without increasing instability. Further runs with smaller smoothing lengths increased instability, and resulting in model crashes or unphysical voids appearing. The results are compared to the numerical results of Greenhow and Moyo (1997) at comparable time steps.

Figure 10 shows good correlation with the numerical results, predicting the fluid height over the rising cylinder correctly. The RMSE error of the fluid above the cylinder is 1.25% with a 0.65% error across the whole surface in the first panel, 0.32% above the cylinder and 0.54% over the whole surface in the second image. The general shape is well matched by both frames, and the error level reduces as the cylinder progresses further to the free surface.

When considering true motion of the cylinder through the fluid, it is important to consider a cylinder whose movement, resulting from the fluid forces, is unbounded. In the following case, a cylinder of the same diameter as the previous test was given a density of 250kgm^{-3}, and initially set up with its centre 1.0m below the still water

surface which was at 1.5m. The particle size was 0.0175m, providing a domain with a total number of particles slightly exceeding 14,500, and the simulation was run using a cubic-spline kernel of smoothing length 0.84, with a Laminar & SPS viscosity value of $1x10^{-6}$.

A velocity vector plot of the test case is displayed in Figure 11. The images show the obstacle as it moves at a constant speed, as it breaches the free surface, and as it reaches its maximum elevation. When observing the images, it is important to note that a side-effect of the SPH method is that when a fluid particle becomes separated from the rest of the domain by a distance greater than the smoothing length *2h*, having no additional particle interactions will cause it to be only affected by gravity. In some cases, this can cause a particle rejoining the fluid to have a disproportionate effect on the domain at the point of impact.

The top vector plot within Figure 11 clearly shows the water flowing around the cylinder in a similar manner as is predicted for the test with a controlled cylinder movement. The fluid on top of the cylinder moves upwards at the same speed as the cylinder and outwards where there is no water forces to prevent this. The space left by the cylinder is quickly filled with water flowing down and inwards from the sides of the obstacle, creating the eddies that can be seen propagating through the sequence of images.

A slight asymmetry can be observed in the results, and is due to the discrete nature of SPH, whereby the particles are not aligned with the central axis, and subsequently the fluid response varies to a degree laterally. Decreasing the particle size would reduce the asymmetric response; however it also increases the potential instabilities within the model.

The middle image shows the beginning of a slight asymmetry to the numerical solution, showing a lower jet flow under the obstacle on the left hand side compared to the right. The water surface over the top of the obstacle is still symmetrical.

The final image shows the cylinder at its maximum elevation. The remaining particles of water are being shed over the obstacle, and the residual eddies below the cylinder can be clearly seen. These eventually cease and the fluid domain enters a state of equilibrium.

4.0 CONCLUSIONS AND DISCUSSION

In this paper we have described the development of WCSPH to include the behaviour of modelling floating object movement as a response to hydrodynamic forces within a fluid domain. This was achieved with an adaption to the WCSPH model that allowed floating objects to be defined and modelled. Phenomena that are traditionally complex to simulate correctly, such as surface piercing and impact pressure of object entry and exit have been modelled successfully. In particular, this paper has examined the water impact, hydrodynamic forces, fluid motions and

movement of objects in the typical case studies of object entry and exit from still water. These case studies show that SPH is a viable method to study floating objects. This work forms a solid grounding for exploring the design and modelling of floating objects using SPH, including wave energy capture devices.

The new object modelling code is based on a system of two different timesteps for each method within the simulation. The water response to the movement is calculated within the original kernel in each time step, and the obstacle movement as a result of the fluid response is computed after this using a distinct kernel function. This has been validated using wedge and cylinder entry, as well as cylinder exit. Initially considering forced plunging of a wedge into the fluid domain, the fluid free surface and movement agrees well with the experimental results of Greenhow and Lin (1983).

Computed values of object velocities and fluid forces have been well predicted for the case of a free wedge slamming into still fluid, and the pressure within the fluid domain also shows good agreement with the results of Shao (2009). Slamming coefficients of wedges of different geometries tend towards the expected theoretical values (Greenhow 1987).

Cylinder entry into still water has been investigated, and the fluid response as well as the dynamic response of the cylinder is well predicted, as compared to experimental and numerical techniques (Zhu et al. 2007). Investigation into cylinder rise has shown that the WCSPH method predicts free surface deformation well, compared to previous results (Greenhow and Moyo 1997; Zhang et al. 2010).

To fully explore the potential opportunities of the SPH method, more research of this phenomena could be pursued. Further work opportunities include more detailed modelling of single or multiple objects within the fluid domain, and air-water interaction within SPH (Rogers et al. 2009).

SPH is a computationally intensive method of modelling, however all tests were completed on a single core of a 2.4GHz processor of a standard desktop computer, with run times less than 40 hours. Further developments currently underway are progressing towards a version of SPH which will run on the Graphics Processing Unit (GPU) of a computer, and will dramatically reduce the time of computations and should allow for significantly higher resolution modelling (Hérault et al. 2010).

ACKNOWLEDGEMENTS

The authors would like to acknowledge the support of the Flood Risk from Extreme Events (FREE) Program of the UK Natural Environment Research Council (NERC) (Grant No. NE/E002129/1) during this project. The authors would also like to acknowledge the support of the South West of England Regional Development Agency through Peninsular Research Institute for Marine Renewable Energy (http://www.primare.org).

REFERENCES

Ataie-Ashtiani, B., and Mansour-Rezaei, S. (2009). "Modification of Weakly Compressible Smoothed Particle Hydrodynamics for Preservation of Angular Momentum in Simulation of Impulsive Wave Problems." *Coastal Engineering Journal*, 51(4), 363-386.

Borg, S. F. (1959). "The Maximum Pressures and Total Force on Straight-Sided Wedges with Small Deadrise." *Journal of the American Society for Naval Engineers*, 71(3), 559-562.

Campbell, J. C., Vignjevic, R., and Patel, M. (2008). "A Coupled Fe-Sph Approach for Simulation of Structural Response to Extreme Wave and Green Water Loading." Offshore Technology Conference, Houston, Texas.

Chaniotis, A. K., Poulikakos, D., and Koumoutsakos, P. (2002). "Remeshed Smoothed Particle Hydrodynamics for the Simulation of Viscous and Heat Conducting Flows." *Journal of Computational Physics*, 182, 67-90.

Cointe, R. (1987). "Two-Dimensional Water-Solid Impact." *Journal of Offshore Mech. Artic Eng.*, 111(1), 109-113.

Colagrossi, A., and Landrini, M. (2003). "Numerical Simulation of Interfacial Flows by Smoothed Particle Hydrodynamics." *Journal of Computational Physics*, 191(1), 448-475.

Dalrymple, R. A. (2007). "Using Smoothed Particle Hydrodynamics for Waves." Asian and Pacific Coasts, Nanjing, China.

Dalrymple, R. A., Gomez-Gesteira, M., Rogers, B. D., Panizzo, A., Zou, S., Crespo, A. J. C., Cuomo, G., and Narayanaswamy, M. (2009). "Smoothed Particle Hydrodynamics for Water Waves." Advances in Numerical Simulation of Nonlinear Water Waves, Q. Ma, ed.

Dalrymple, R. A., and Rogers, B. D. (2006). "Numerical Modeling of Water Waves with the Sph Method." *Coastal Engineering*, 53, 141-147.

Dyka, C. T., and Ingel, R. P. (1995). "An Approach for Tension Instability in Smoothed Particle Hydrodynamics (Sph)." *Computers & Structures*, 57(4), 573-580.

Dyka, C. T., Randles, P. W., and Ingel, R. P. (1997). "Stress Points for Tension Instability in Sph." *International Journal for Numerical Methods in engineering*, 40(13), 2325-2341.

Fang, J., Parriaux, A., Rentschler, M., and Ancey, C. (2009). "Improved Sph Methods for Simulating Free Surface Flows of Viscous Fluids." *Applied Numerical Mathematics*, 59, 251-271.

Ferrari, A. (2010). "Sph Simulation of a Free Surface Flow over a Sharp-Crested Weir." *Advances in Water Resources*, 33, 7.

Ferrari, A., Dumbser, M., Toro, E. F., and Armanini, A. (2009). "A New 3d Parallel Sph Scheme for Free Surface Flows." *Computers & Fluids*, 39, 1203-1217.

Gómez-Gesteira, M., Cerqueiro, D., Crespo, C., and Dalrymple, R. A. (2005). "Green Water Overtopping Analyzed with a Sph Model." *Ocean Engineering*, 32(2), 223-238.

Gómez-Gesteira, M., and Dalrymple, R. A. (2004). "Using a 3d Sph Method for Wave Impact on a Tall Structure." *Journal of Waterway, Port, Coastal and Ocean Engineering*, 130(2), 63-69.

Gómez-Gesteira, M., Rogers, B. D., Dalrymple, R. A., and Crespo, A. J. C. (2010). "State-of-the-Art of Classical Sph for Free Surface Flows." *Journal of Hydraulic Research*, 48(extra), 6-27.

Gong, K., Liu, H., and Wang, B.-l. (2009). "Water Entry of a Wedge Based on Sph Model with an Improved Boundary Treatment." *Journal of Hydrodynamics*, 21(6), 750-757.

Greenhow, M. (1987). "Wedge Entry into Initially Calm Water." *Applied Ocean Research*, 9(4), 214-223.

Greenhow, M. (1993). "A Complex Cariable Method for the Floating-Body Boundary-Value Problem." *Journal of Computational and Applied Mathematics*, 46, 115-128.

Greenhow, M., and Lin, W. M. (1983). "Non-Linear Free Surface Effects: Experiments and Theory." Rep. No. 83-19 Department of Ocean Engineering, MIT, Cambridge.

Greenhow, M., and Moyo, S. (1997). "Water Entry and Exit of Horizontal Circular Cylinders." *Phil. Trans. Roy. Soc. Lond.*, 335(A), 551-563.

Gringold, R., and Monaghan, J. J. (1997). "Smoothed Particle Hydrodynamics: Theory and Application to Non-Spherical Stars." *Monthly Notices of the Royal Astronomical Society*, 181, 375-388.

Hérault, A., Bilotta, G., and Dalrymple, R. A. (2010). "Sph on Gpu with Cuda." *Journal of Hydraulic Research*, 48(extra), 6-27.

Judge, C., Troesch, A., and Perlin, M. (2004). "Initial Water Impact of a Wedge at Vertical and Oblique Angles." *Journal of Engineering Mathematics*, 48(1), 279-303.

Kleefsman, K. M. T., Fekken, G., Veldman, A. E. P., Iwanowski, B., and Buchner, B. (2005). "A Volume-of-Fluid Based Simulation Method for Wave Impact Problems." *Journal of Computational Physics*, 206, 363-393.

Lucy, L. (1997). "A Numerical Approach to Testing of the Fusion Process." *Astronomical Journal*, 88, 12.

Molteni, D., and Colagrossi, A. (2009). "A Simple Procedure to Improve the Pressure Evaluation in Hydrodynamic Context Using Sph." *Computer Physics Communications*, 180, 861-872.

Monaghan, J. J. (1989). "On the Problem of Penetration in Particle Methods." *Journal of Computational Physics*, 82(1), 1-15.

Monaghan, J. J. (1994). "Simulating Free Surface Flows with Sph." *Journal of Computational Physics*, 110, 399-406.

Monaghan, J. J. (2000). "Sph without a Tensile Instability." *Journal of Computational Physics*, 159, 290-311.

Morris, J. P. (1996). "Analysis of Sph with Applications," PhD Thesis. Mathematics Department, Monash University, Melbourne, Australia.

Oger, G., Doring, M., Alessandrini, B., and P, F. (2006). "Two Dimensional Sph Simulations of Wedge Water Entries." *Journal of Computational Physics*, 213(1), 803-822.

Rogers, B. D., Dalrymple, R. A., and Stansby, P. K. (2008). "Sph Modelling of Floating Bodies in the Surf Zone." ICCE, Hamburg.

Rogers, B. D., Leduc, J., Marongiu, J.-C., and Leboeuf, F. "Comparison and Evaluation of Multi-Phase and Surface Tension Models." *4th SPHERIC Workshop*, Nantes, France, 30-37.

Shao, S. (2009). "Incompressible Sph Simulation of Water Entry of a Free-Falling Object." *International Journal for Numerical methods in Fluids*, 59(1), 91-115.

Shao, S., Ji, C., Graham, D. I., Reeve, D. E., James, P. W., and Chadwick, A. J. (2006). "Simulation of Wave Overtopping by an Incompressible Sph Model." *Coastal Engineering*, 53(9), 723-735.

Shao, S., and Y.M.Lo, E. (2003). "Incompressible Sph Method for Simulating Newtonian and Non-Newtonian Flows with a Free Surface." *Advances in Water Resources*, 26(7), 787-800.

SPHYSICS. (2008). "Sphysics Home Page" University of Manchester. http://wiki.manchester.ac.uk/sphysics/index.php/Main_Page Accessed 15/10/2007

Vaughan, G. L., Healy, T. R., Bryan, K. R., Sneyd, A. D., and Gorman, R. M. (2008). "Completeness, Conservation and Error in Sph for Fluids." *International Journal for Numerical methods in Fluids*, 56, 37-62.

Viccione, G., Bovolin, V., and Carratelli, E. P. (2008). "Defining and Optimizing Algorithms for Neighbouring Particle Identification in Sph Fluid Simulations." *International Journal for Numerical Methods in Fluids*, 58(6), 625-638.

Wagner, H. (1932). "Uber Stoss-Und Gleitvorgange an Der Oberflache Von Flussigkeiten." *ZAMM*, 12(4), 192-235.

Xu, R., Stansby, P., and Laurence, D. (2009). "Accuracy and Stability in Incompressible Sph (Isph) Based on the Projection Method and a New Approach." *Journal of Computational Physics*, 339, 6703-6725.

Yan, S., and Ma, Q. W. (2007). "Numerical Simulation of Fully Nonlinear Interaction between Steep Waves and 2d Floating Bodies Using the Qale-Fem Method." *Journal of Computational Physics*, 221, 666-692.

Zhang, Y., Zou, Q., Greaves, D., Reeve, D., Hunt-Raby, A., Graham, D. I., James, P. W., and Lv, X. (2010). "A Level Set Immersed Boundary Method for Water Entry and Exit." *Communications in Computational Physics, accepted*, In Press.

Zhao, R., and Faltinsen, O. (1993). "Water Entry of Two Dimensional Bodies." *Journal of Fluid Mechanics*, 246, 593-612.

Zhao, R., Faltinsen, O., and Aarsnes, J. (1997). "Water Entry of Arbitrary Two-Dimensional Sections with and without Flow Separation." Twenty-first Symposium on Naval Hydrdynamics, Trondheim, Norway.

Zhu, X., Faltinsen, O. M., and Hu, C. (2007). "Water Entry and Exit of a Horizontal Circular Cylinder." *Journal of Offshore Mechanics and Arctic Engineering*, 129, 253.

FIGURES

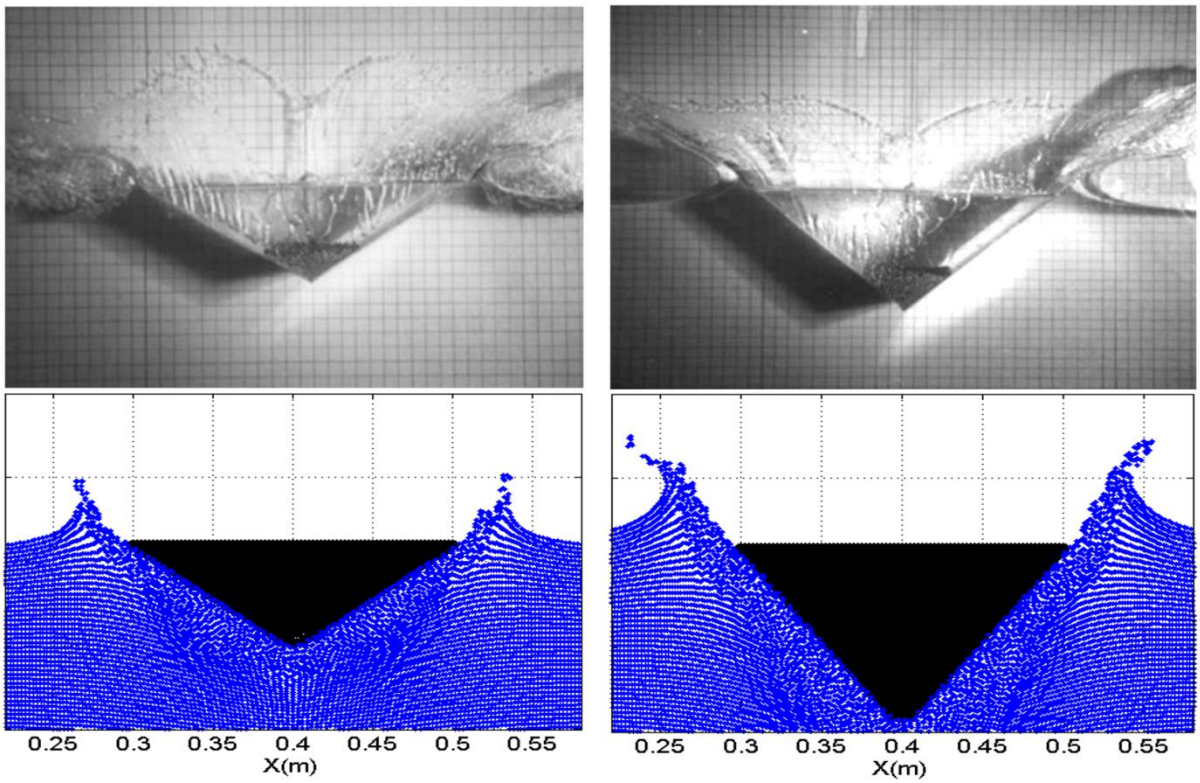

Fig. 1. Comparison of WCSPH (colour) to the experimental results of Greenhow and Lin (1983) for plunging wedges of 30^{o} and 45^{o} deadrise angles at a constant velocity into still water.

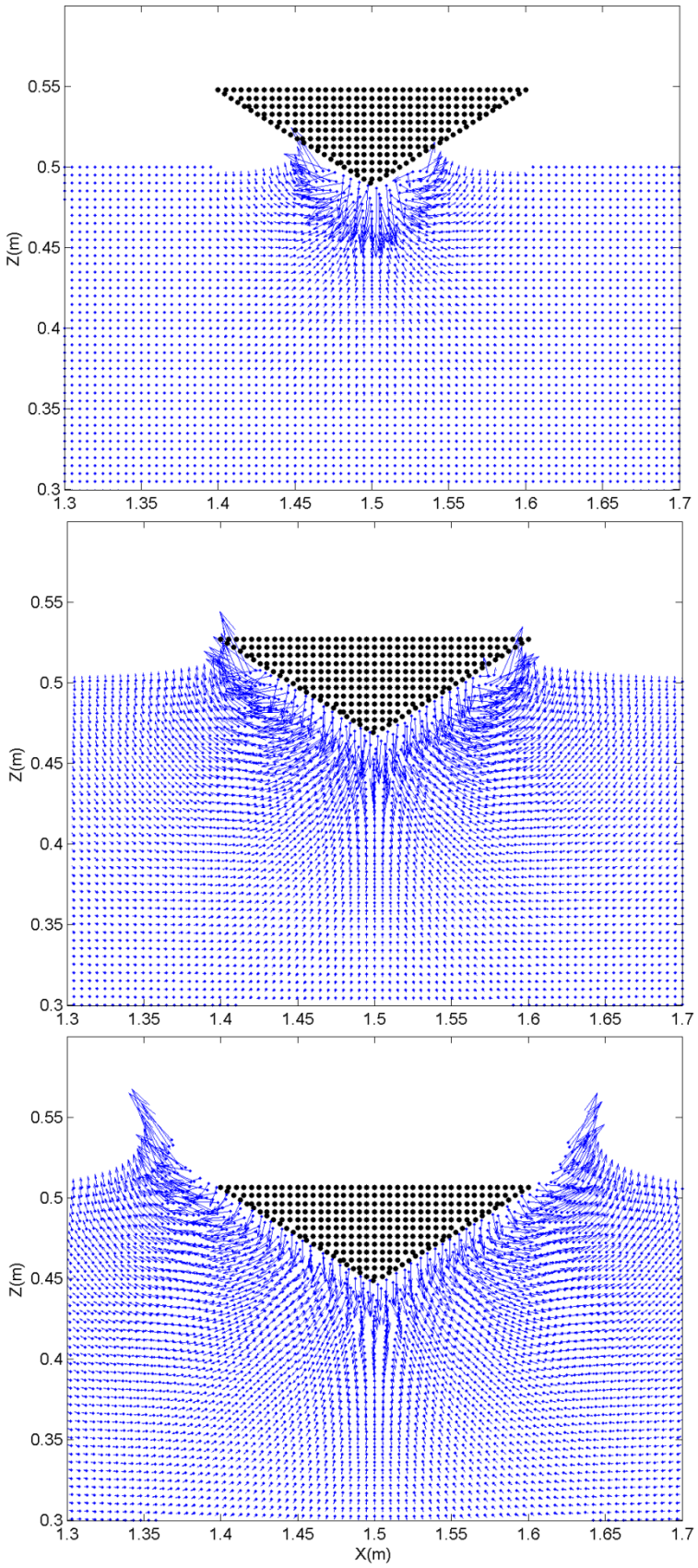

Fig. 2. The velocity vector plots of the fluid domain under impact of a 30^{o} wedge, at 0.004s, 0.016s and 0.02s. The jets as described in Greenhow (1987) can be clearly seen.

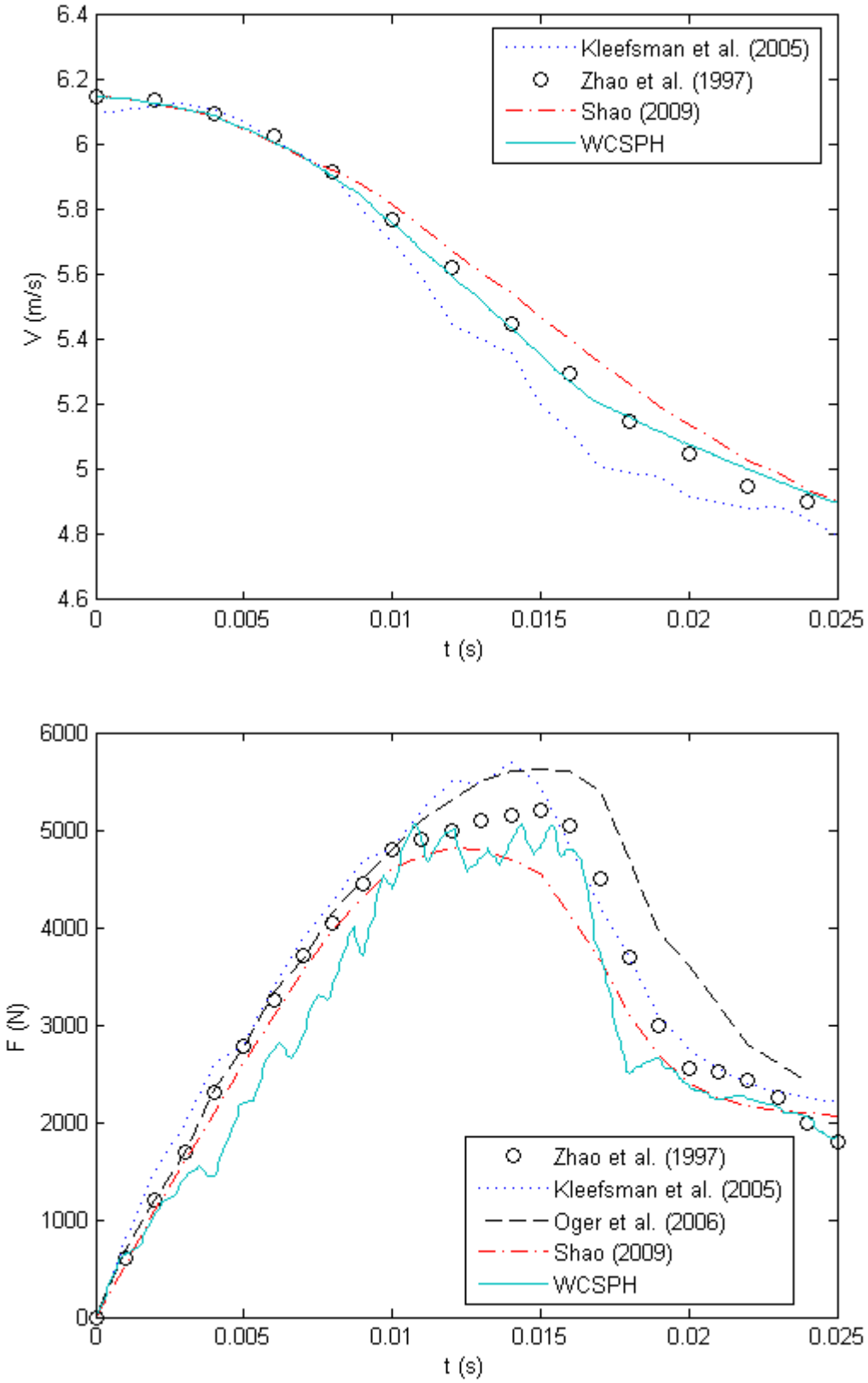

Fig. 3. Top. The falling velocity of a 30^{o} deadrise angle wedge, timed from the moment of entry. Bottom. The vertical force exerted on the wedge by the fluid body.

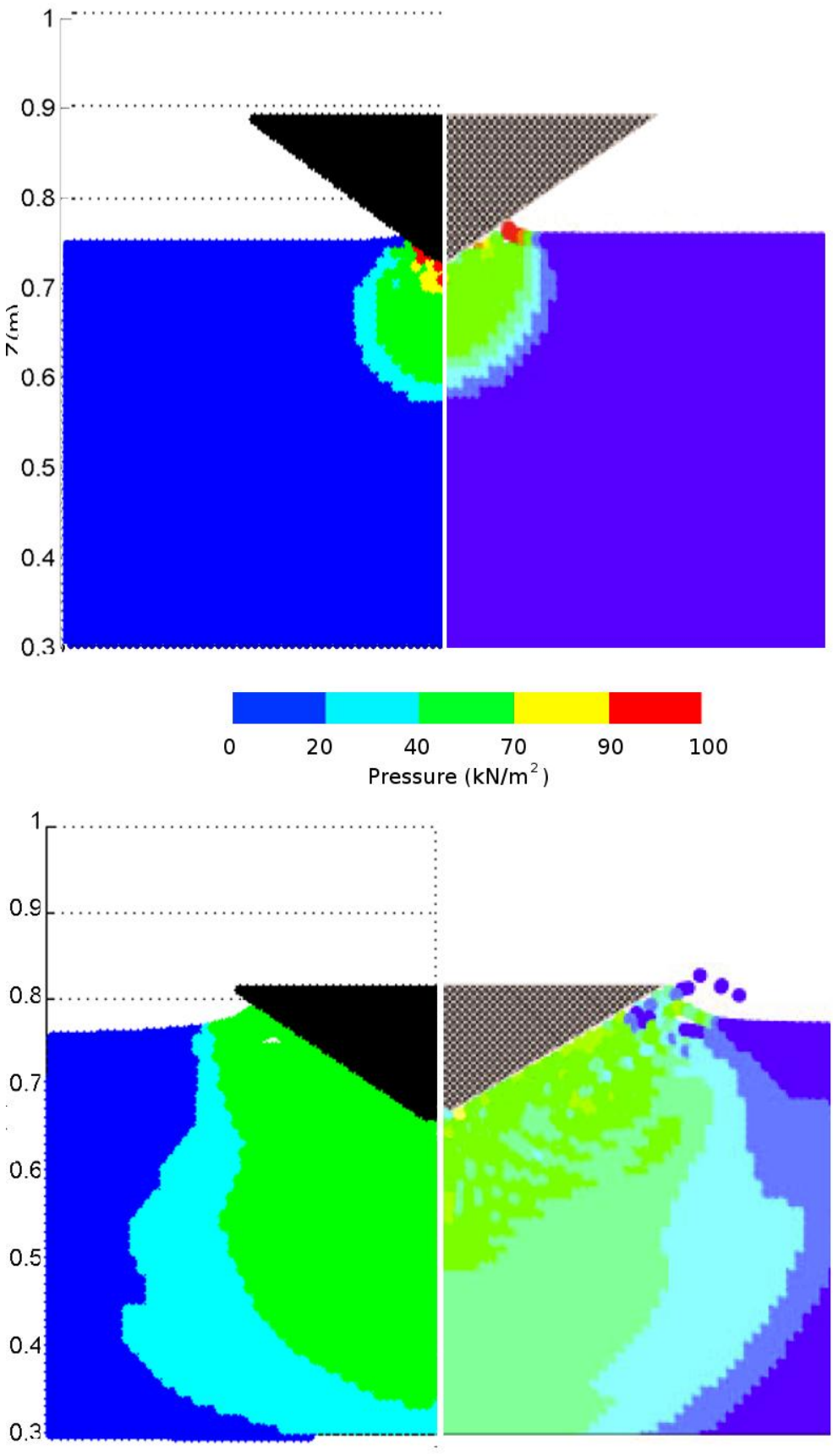

Fig. 4. Pressure under the impact of a 30^o wedge with WCSPH on the left hand side and the ISPH results of Shao (2009) on the right.

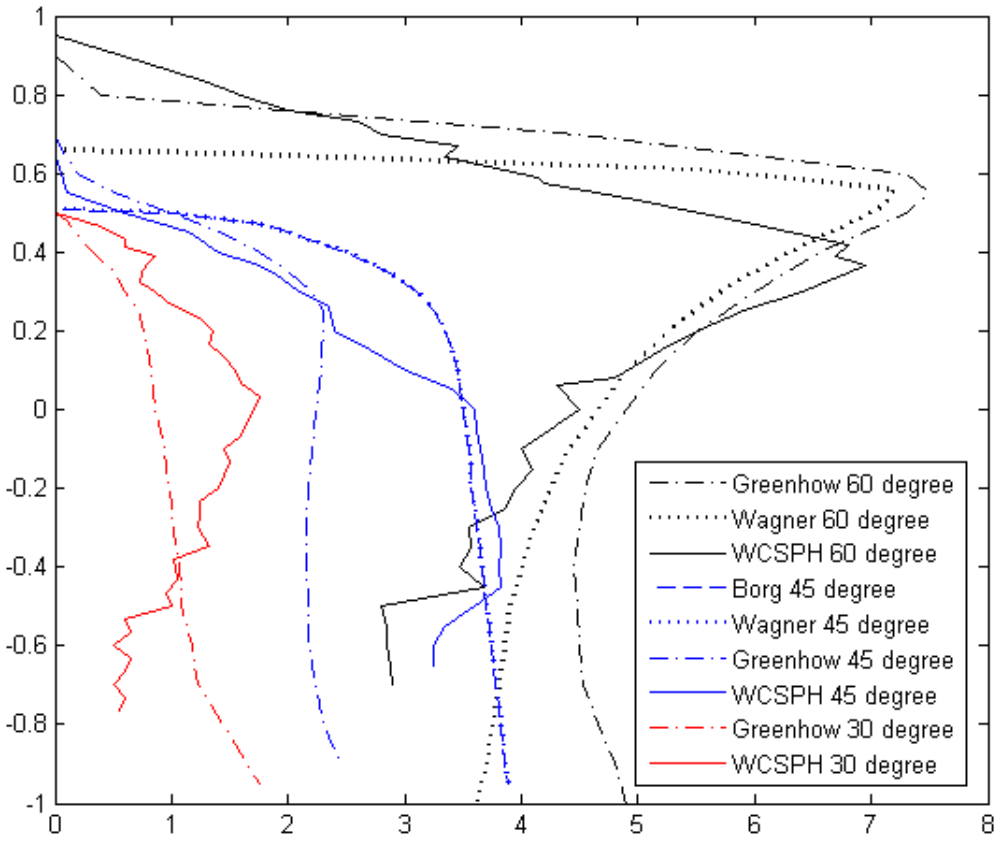

Fig. 5. Slamming coefficient plotted against dimensionless depth for 2D wedges plotted over the predicted values from Greenhow (1987) (dash-dot). Multiple lines for the 60^{o} and the 45^{o} wedges show the theories of Borg (dotted) and Wagner (dashed).

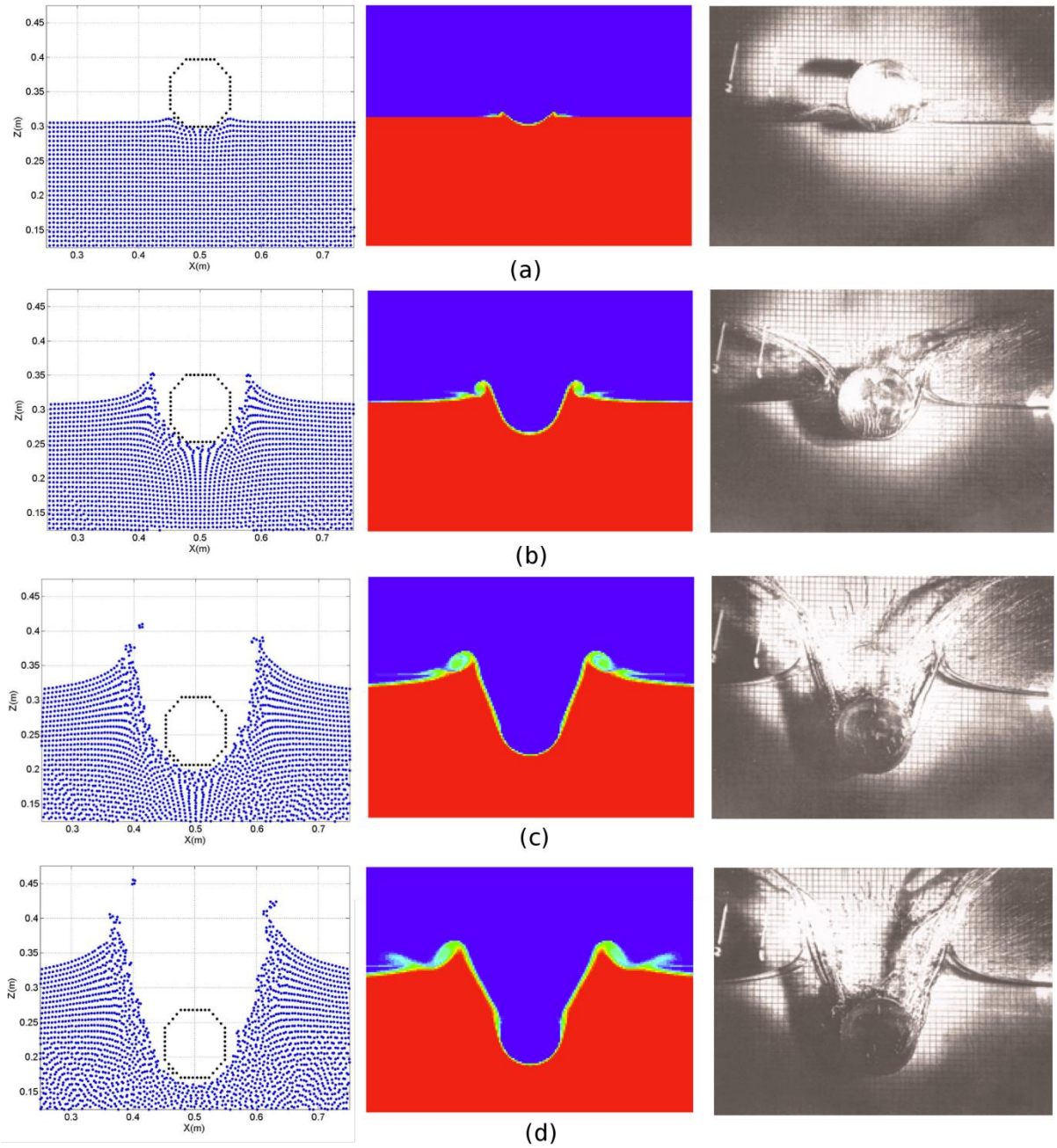

Fig. 6. Free surface deformation during water entry of a cylinder of density 500kgm^{-3}. WCSPH results (left) compared with the model results using CIP by Zhu et al. (2007) (centre) and experimental results of Greenhow and Lin (1983) (right) at times after impact of (a) 0.005s, (b) 0.030s, (c) 0.085s, and (d) 0.120s.

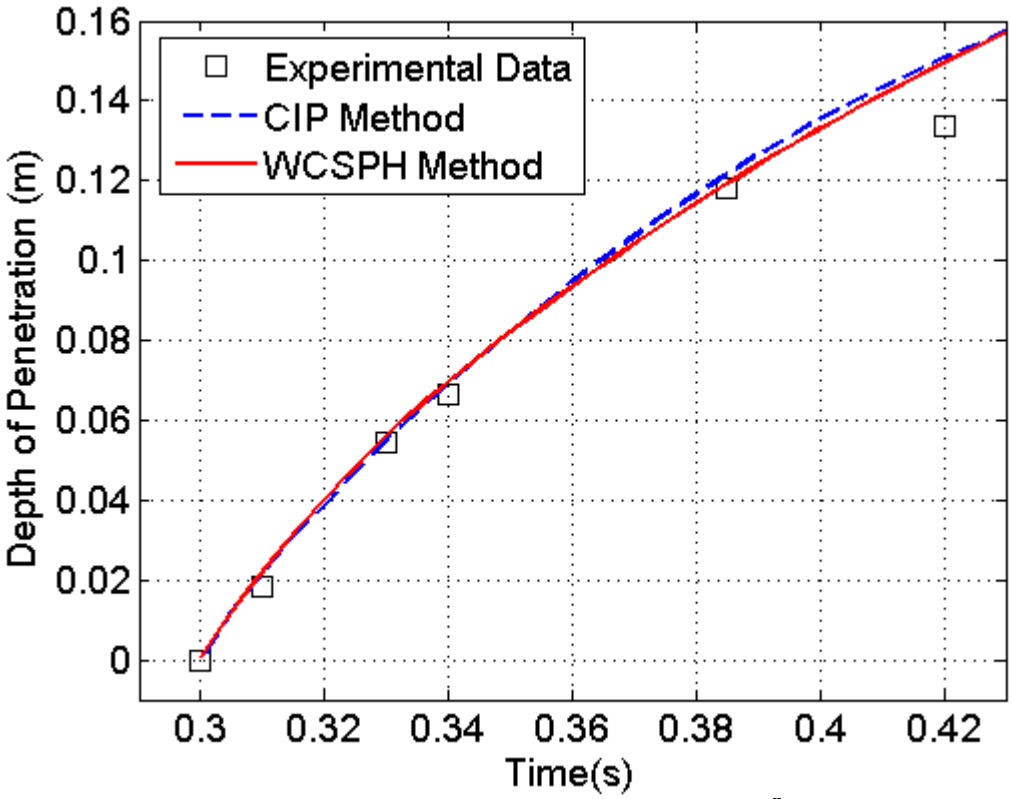

Fig. 7. Depth penetration of a cylinder of density 500kgm^{-3}. WCSPH results (black), blue dashed line shows the model results using CIP by Zhu et al. (2007) and points show the experimental results of Greenhow and Lin (1983).

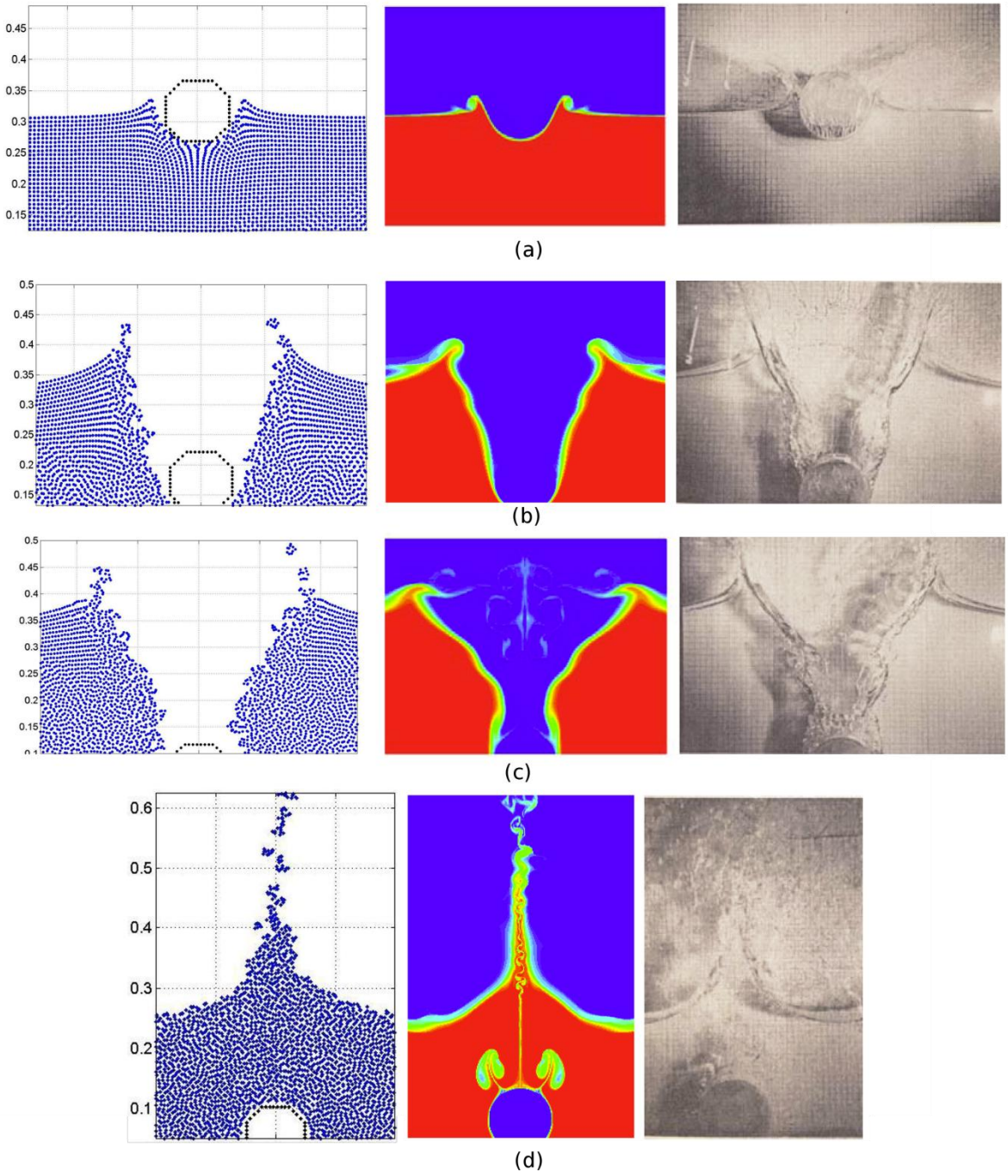

Fig. 8. Free surface deformation during water entry of a cylinder of density 1000kgm^{-3}. WCSPH results (left) compared with the model results using CIP by Zhu et al. (2007) (centre) and experimental results of Greenhow and Lin (1983) (right). Images shown at time after impact of (a) 0.015s, (b) 0.110s, (c) 0.200s, and (d) 0.450s.

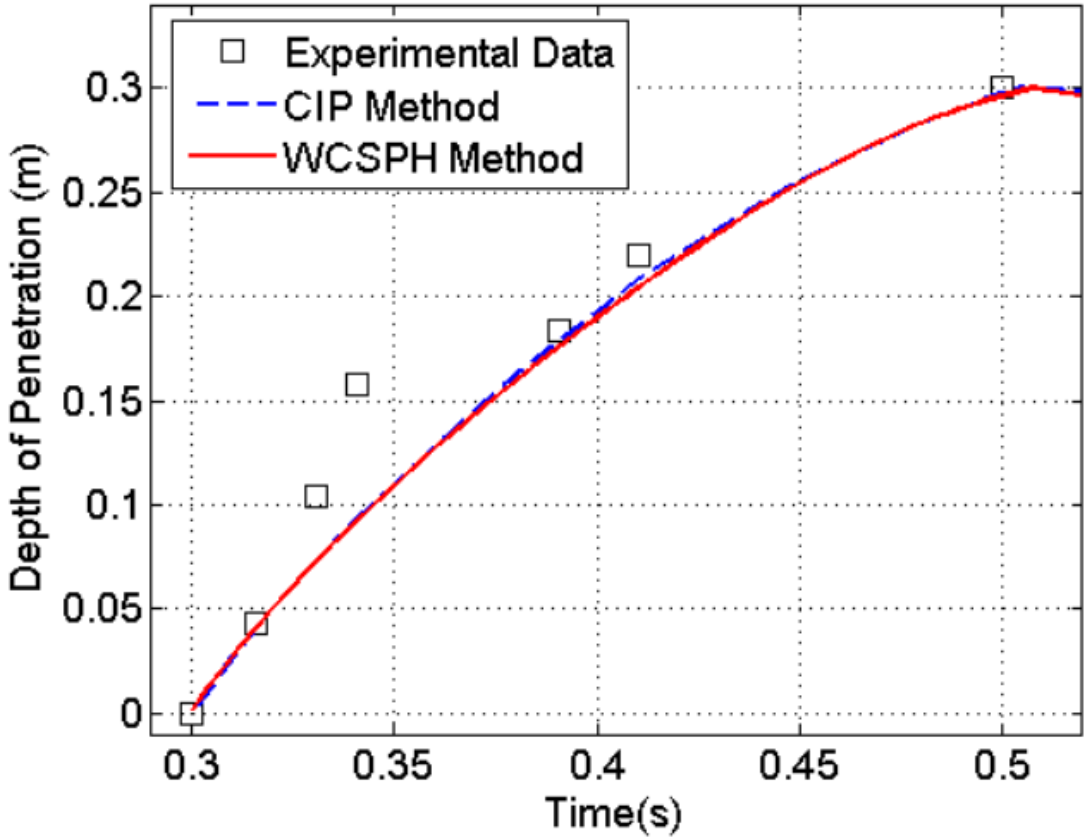

Fig. 9. Depth penetration of a cylinder of density 1000kgm^{-3}. WCSPH results (black), blue dashed line shows the model results using CIP by Zhu et al (2007) and points shows the experimental results of Greenhow and Lin (1983).

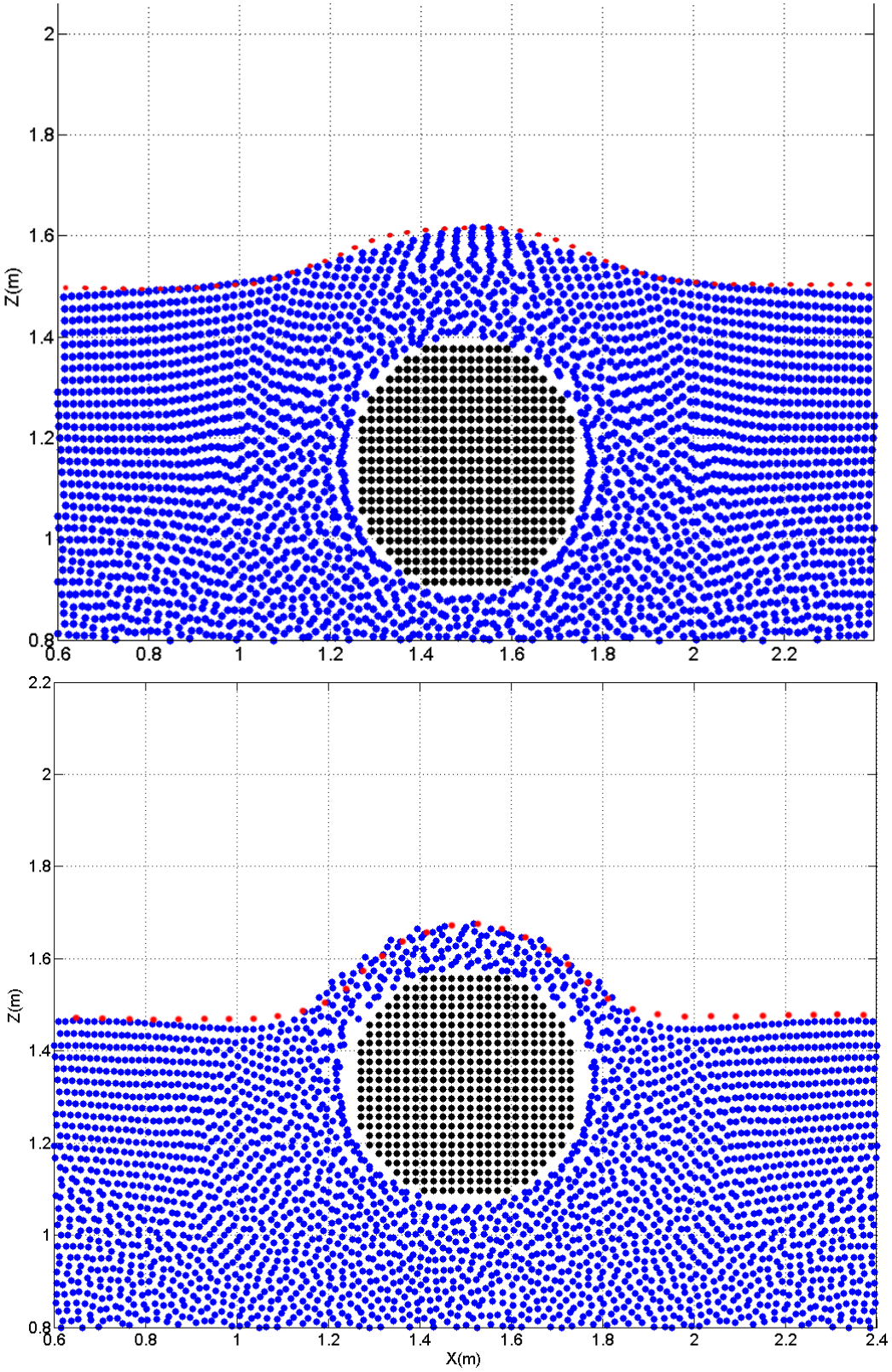

Fig. 10. Free surface deformation due to a forced movement cylinder rising through the free surface, for dimensionless time (t=Ut/d) of 0.4 and 0.6. Red dots show the numerical results presented in Greenhow and Moyo (1997).

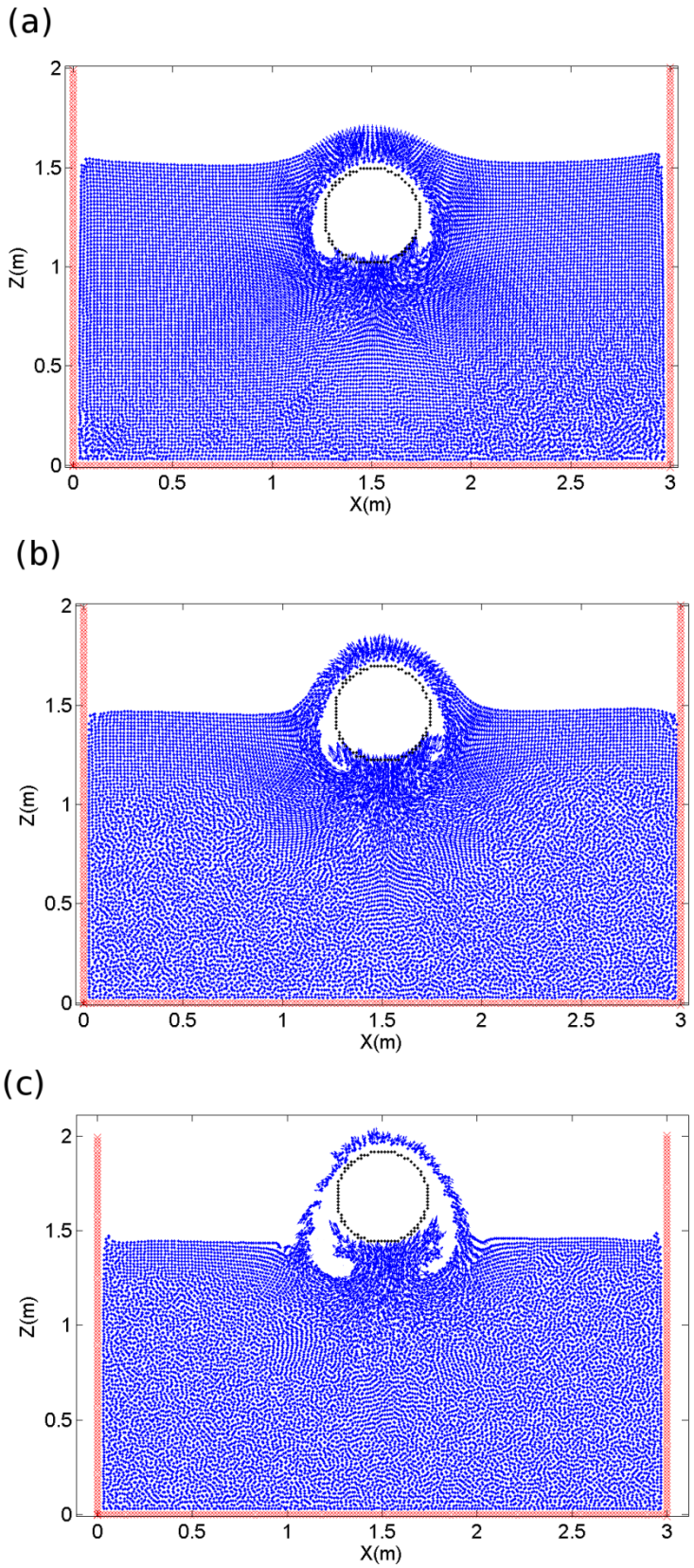

Fig. 11. Velocity plots of the fluid domain as a free movement of a cylinder, of density 250kgm^{-3} (top) rises through the fluid, (middle) aligns with the free surface, and (bottom) reaches maximum elevation.